Turkish Journal of Electrical Engineering & Computer Sciences

http://journals.tubitak.gov.tr/elektrik/

Review Article

Turk J Elec Eng & Comp Sci
(2024) 32: 305 – 319

doi:10.55730/1300-0632.4070

Atomic Comagnetometer Gyroscopes for Inertial Navigation Systems: A Review

Murat Salim KARABİNAOĞLU[1]*, Bekir ÇAKIR[2], Mustafa Engin BAŞOĞLU[3]
[1]TÜBİTAK National Metrology Institute (TÜBİTAK UME), Kocaeli,Turkiye
[2]Department of Electrical Engineering, Kocaeli University,
Kocaeli, Turkiye
[3]Department of Electrical and Electronics Engineering, Faculty of Engineering and Natural Sciences,
Gümüşhane University, Gümüşhane, Turkiye

Received: 24.10.2023 • **Accepted/Published Online:** 08.02.2024 • **Final Version:** 14.03.2024

Abstract: In recent years, developments in quantum sensing, laser, and atomic sensor technologies have also enabled advancement in the field of quantum navigation. Atomic-based gyroscopes have emerged as one of the most critical atomic sensors in this respect. In this review, a brief technology statement of spin exchange relaxation free (SERF) and nuclear magnetic resonance (NMR) type atomic comagnetometer gyroscope (CG) is presented. Related studies in the literature have been gathered, and the fundamental compositions of CGs with technical basics are presented. A comparison of SERF and NMR CGs is provided. A basic simulation of SERF CG was carried out because of its high theoretic bias stability limit. Besides, some highly critical challenges for CGs were examined and reported with compensation methods. The objective of this review is to offer a guide for researchers to develop high-precision atomic gyroscopes and to encourage further research.

Key words: Inertial navigation, atomic sensor, comagnetometer gyroscope, SERF CG

1. Introduction

Inertial navigation systems (INSs) have become an interesting topic in recent years, with the potential to provide navigation in cases where the navigation systems are not working properly or are blocked [1]. In contrast to GNSS, which provides an absolute position, INSs provide a relative position based on the initial point. In addition, an INS containing an atomic sensor can be given as an example of the passive quantum navigation system. Since these sensors are closed to the outside world and autonomous, they can provide high reliability and applicability [2]. Thus, they have the potential to be used on many critical platforms in the defense industry, including nuclear submarines [2].

The inertial measurement unit (IMU) used in INSs is usually composed of gyroscopes and accelerometers and is used to determine the rate of rotation and acceleration of an inertial reference [3]. Gyroscopes have many kinds of applications, such as inertial navigation, gravitational wave detection, etc. [4–7]. Researchers have classified atomic-based gyroscopes into two subcategories: atomic interference gyroscope (AIG) and atomic spin gyroscope (ASG) [8]. AIG is named "cold atom gyroscope" which uses various atomic interference effects to sense rotation [9, 10]. ASG can also be categorized as NMR and SERF-type gyroscopes [8]. Developments in quantum sensing [11] provide researchers with physically small, low-cost, and highly sensitive NMR gyroscopes

*Correspondence: murat.karabinaoglu@tubitak.gov.tr

[12]. NMR and SERF-type gyroscopes are also examples of CG which was first discovered by a team at Princeton University in 2005 [13].

Table 1 shows the comparison of NMR and SERF-type gyroscope technologies [8]. The theoretical bias stability limits of NMR and SERF CG are $10^{-4}\,^{\circ}/h$ and $10^{-8}\,^{\circ}/h$, respectively [8]. Northrop Grumman Corporation's micro NMR CG has a volume of 5 cm^3 and a bias stability of 0.02 °/h in this respect [14, 15]. On the contrary, it is known from the literature that only some experimental samples exist as SERF CG [16]. This extraordinary sensitivity potential of SERF CG is our main reason for choosing this structure [13, 17, 18].

Table 1. Atomic spin comagnetometer gyroscopes [13].

Characteristics	NMR CG	SERF CG
Sensing principle	Nuclear spin	Electron spin
Size	Small	Small
Theoretical bias stability ($/h$)	10^{-4}	10^{-8}
Practical bias stability ($/h$)	10^{-2}	10^{-5}
Alkali type	Cs, Rb, K	Cs, Rb, K
Buffer/noble gas	N, ^{3}He, ^{21}Ne, ^{129}Xe, ^{131}Xe	^{3}He, ^{21}Ne, ^{129}Xe
Power consumption	Relatively low	Relatively high
Field compensation mechanism	Two nuclear spins	Self compensation
Status	End user product	Prototype

It is expected that SERF CG will be used in inertial navigation systems as a new generation of inertial measurement units shortly [19]. CG has a promising potential for highly accurate and compact gyroscopes for future inertial navigation applications by using microfabrication methods developed for atomic clocks [20]. A feasibility report similar to this study was published in 2021 and examined atomic gyroscope strategies based on NMR and SERF [21]. The contributions of this article are; an introduction to quantum navigation sensors and a comparison of atomic spin gyroscope types, technical fundamentals, and a basic simulation of SERF CGs, an examination of the basic compositions and some challenging issues of SERF CGs, and a presentation of a review of SERF CGs for researchers for further advanced research. The arrangement of the paper is as follows. Section 2 consists of the research and development with applications of CG technology. Section 3 gives the technical basics and the simulation of a SERF CG. In Section 4, the fundamental compositions of CGs are reported. In Section 5, some challenges for the CGs are described briefly, and the compensation methods for the errors are explained in detail.

2. Research and development with applications

Recent advances in quantum sensing and quantum sensors are quite remarkable [11] such as in time-frequency [22], magnetic and electric fields [23] rotation [13, 24], and temperature [25] sensing. The use of polarized gases in inertial sensors to detect rotation is preferred for the following reasons: low internal noise, miniaturization possibilities, low power consumption, insensitivity to acceleration, and independence from experimental parameters [26]. It has been determined empirically that if enough spin-exchange collisions are created in the vapor cell, it can slow down the Larmor frequency and narrow the linewidth of magnetic resonance, depending on the alkali metal vapor density [27]. Happer and his group showed how the spin exchange affects magnetic resonance linewidth and demonstrated that spin exchange broadening can be eliminated in the presence of a high vapor

density of $10^{13}/cm^3$ and a low magnetic field [28]. The basic working principle of the SERF regime is based on the observation of suppression of spin relaxation due to collisions in alkali metal vapor [27, 29, 30]. Alkali metal atoms can effectively polarize noble gas atoms by suppressing spin exchange relaxation in the SERF regime. This led to the creation of the SERF magnetometer in 2002 and also to the SERF CG technology soon. When CG was first discovered, the ^{3}He-K CG was reported to have 2x10^{-3} $^\circ/h^{1/2}$ angle random walk (ARW) and 4x10^{-2} $^\circ/h$ bias stability [13]. Subsequently, rotation sensitivities of 2.5x10^{-7} $^\circ/h$ and 1.8x10^{-7} $^\circ/h$ were presented, respectively [31, 32]. CG can be used in inertial navigation [13, 14, 33], dark matter research [34], Lorentz invariance violations [32], etc. It may therefore make an excellent gyroscope for navigation because it has a high degree of sensitivity for detecting the precession of noble gas atoms [14, 35, 36].

3. Technical basics and simulation

3.1. Technical basics

The atomic vapor cell of SERF CG consists of two or more species, each of which experiences the same magnetic field but has a different magnetic response because of their unique gyromagnetic ratios [13]. Nuclear spins (P^n) and electron spins (P^e) are both used in CG to sense rotation [13]. A group of Bloch equations [37] can be utilized to explain the evolution of the SERF CG dynamics and the P^e and P^n polarizations of CG in Equation (1) [13].

$$\begin{aligned}\frac{\partial P^e}{\partial t} &= \frac{\gamma_e}{Q}\left(B+\lambda M^n P^n + L\right)\times P^e + \Omega \times P^e \\ &\quad + \left(R_p s_p + R_{se}^{en} P^n - R_{tot}^e P^e\right)/Q\end{aligned} \tag{1}$$

$$\frac{\partial P^n}{\partial t} = \gamma_n\left(B+\lambda M^e P^e\right)\times P^n - \Omega \times P^n + R_{se}^{ne} P^e - R_{tot}^n P^n \tag{2}$$

Here, $\lambda M^n\ P^n\,(B^n)$ and $\lambda M^e\ P^e\,(B^e)$ are the magnetic fields that nuclear spin and electron spin actually experience because of the other species' polarization, λ is the wavelength, P^n and P^e are polarizations and λM^n and λM^e are magnetizations of nuclear spin and electron spin, respectively. Besides, R_{tot}^e and R_{tot}^n are total relaxation rates, R_{se}^{en} and R_{se}^{ne} are pumping rates for electron and nucleus. Besides, L and B represent the net light shift and magnetic field experienced by electrons, R_p is the pumping rate of the pump laser, s_p is the polarization of pump photons, Q represents the slowing down factor and Ω is the inertial rotation rate. Equation (1) shows the time-dependent evolution of coupled atomic spin ensembles in the atomic comagnetometer. The external magnetic field applied to the system, indicated by B in Equation 1, enables the electron and nucleus to experience different magnetic fields.

Figure 1 shows the basic working principle of SERF CG. Here, B^e and B^n represent the magnetic fields of the electron and nucleus, respectively. B^c is the applied compensation field which was calculated using B^e and B^n as shown in Figure 1a. B^c is also applied in the z-axis direction and is explained in detail in the next section. Figure 1a illustrates the utilization of the pump and probe lasers in the z and x directions. When the inertial rotation is applied to the system in Figure 1b, the nuclear spins respond by emitting a precession signal. Noble gas magnetization in CG follows fluctuations in the low-frequency magnetic field. To compensate for the fields generated by electron and nuclear magnetization, a biased magnetic field (B^c) parallel to the pump light is applied [13]. Due to the applied magnetic field, slight changes in the external magnetic field can be adiabatically canceled by the atoms of noble gases. Since atoms may balance themselves, the operating point

can also be referred to as the compensation point and the alkali metal atoms are subjected to a stabilizing magnetic field that is in opposition to the direction of their magnetization [38, 39]. It should be noted that this compensation mechanism can work efficiently up to a certain bandwidth limit. It is presented that the transient response given inertial rotation is the fastest when the pumping rate is equal to the product of the effective gyromagnetic ratio and the electron spin polarization field factor [38]. Alkali metal atoms are not affected by magnetic field changes because the transverse magnetization of the noble gas cancels the drift in the magnetic field [13].

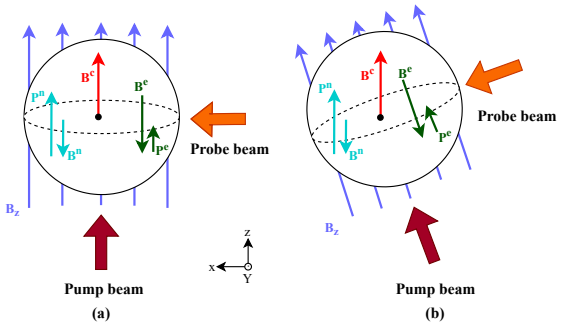

Figure 1. SERF CG polarizations.

Nuclear spins in CGs have a self-compensating mechanism that can suppress transverse magnetic field fluctuations that are parallel to the probe laser direction rather than in its direction [20]. Figure 2 depicts a simplified illustration of the configuration of a typical CG experimental setup. Using the proper optical components, the pump and probe lasers are configured for circular and linear polarization in a perpendicular orientation, respectively. The magnetic field of the Earth is attenuated by the factor 10^3-10^6 using a multilayer Mu-metal shielding unit [40]. Here, $\lambda/2$ is a half-wave plate, $\lambda/4$ is a quarter-wave plate, PD is a photodiode, PBS is a polarization beam splitter and NE is a noise eater in Figure 2. Using a circularly polarized pump beam, alkali metal atoms in the vapor cell are polarized along the z-axis. Then, to measure the polarization component along the x-axis, a probe beam that is linearly polarized is used. The appropriate heater and temperature-sensing components are assembled in the boron-nitride oven to provide the atomic vapor cell with the necessary temperature conditions. The multiaxial magnetic field coils handle not only the necessary DC and AC magnetic fields but also the cancellation of residual magnetic fields. The probe beam traversing the vapor cell is sent to the photodetectors with the use of PBS, providing a balanced light detection technique. As a result, the light energy is transformed into electrical energy and sent to the Lock-In. After that, signal processing and rotation data capture steps are carried out.

3.2. Simulation

Figure 1 shows that the electron and nucleus polarization components P^e ($P^e = P^e_x + iP^e_y$) and P^n ($P^n = P^n_x + iP^n_y$) in the longitudinal axis which was given in Equation (1) and can be assumed to be constants [41, 42]. The response of the comagnetometer is obtained from the electron polarization component in the direction of the probe laser in the experimental setup given in Figure 2.

$$P^e_x = \frac{P^e_z K^2 \Omega}{1 + K^2 \Omega^2} \tag{3}$$

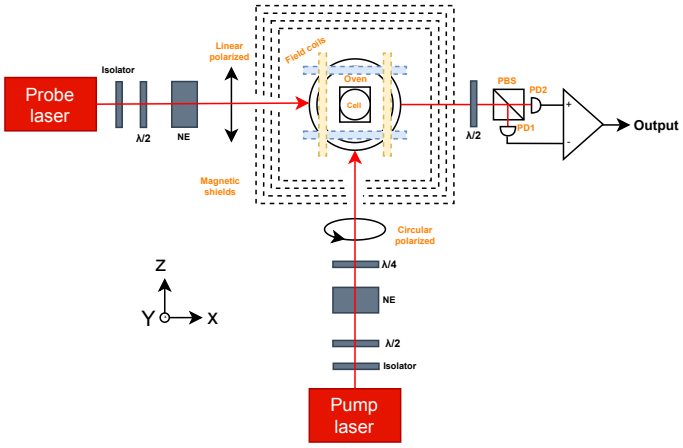

Figure 2. Experimental setup scheme.

When the dynamics of a SERF-type comagnetometer are analyzed, P_x^e polarization depends on the Ω rotation rate, which is given in Equation (3) [38]. Here, the K coefficient in Equation (3) is used to facilitate mathematical calculations and is defined in Equation (4).

$$K = \frac{\gamma_e \gamma_n \left(B^n\right)^2 R_{tot}^e}{\gamma_e B^n R_{tot}^e + \gamma_e B^e R_{tot}^n} \tag{4}$$

In addition, $B^e = \lambda M^e P^e$ and $B^n = \lambda M^n P^n$ represent the Fermi contact interactions during the spin exchange of electron and nucleus, respectively. Here, M^e and M^n are the magnetizations of electron and nuclear spins. The λ is defined as $\frac{8\pi K_0}{3}$. Here, K_0 is also defined as the spin exchange enhancement factor [43]. In CG, the magnetization caused by the spins of the electron and nuclear atoms is canceled by an external compensating magnetic field B^c. A definition of B^c is given in Equation (5). If B^c is equal to the opposite sign of the sum of B^e and B^n, the magnetization produced by nuclear and electron spin polarization can be compensated.

$$B^c = -B^e - B^n \tag{5}$$

$$P_z^e = \frac{R_p}{R_p + R_{rel}} \tag{6}$$

Besides, the electron polarization in the z-axis direction is given in Equation (6) [38]. Here, the electron spin relaxation rate is represented by R_{rel}. The response of a comagnetometer to inertial rotation can be determined using the equation (3). The parameters: B^e = 30 nT, B^n =110 nT, γ_e=28 Hz/nT, γ_n =3.36x10^{-3} Hz/nT, R_{tot}^e = 23.84 s^{-1}, R_{tot}^n = 0.12 s^{-1}, R_{rel} = 500.5 s^{-1}, R_p =0$\cdots$3000 s^{-1}. For this purpose, a simulation was carried out to find out the effect of inertial rotation on the CG output signal using the parameters above. It was created for this paper and inspired by various papers in the literature [38, 41, 44].

Figure 3 shows the simulation result using these parameters and how the P_x^e polarization at the output of the comagnetometer changes depending on the inertial rotation input Ω. The basic dispersion graph of the

polarization change in case the comagnetometer rotates at -5 and +5 rad/s speed is shown with this simulation. Thus, basic information on how the phase and amplitude of the gyroscope dispersion output can change within the scope of different magnetic fields, gyromagnetic ratio, relaxation, and pumping rates are given. In addition, this study can be used for further research by differentiating the relevant parameters.

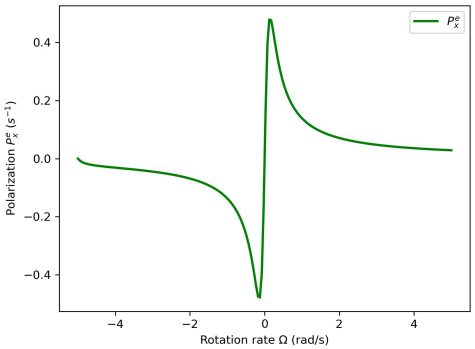

Figure 3. SERF CG response due to change in rotation rate.

4. Fundamental compositions

The composition used in SERF CG may vary depending on the research team and is summarized in Table 2. Depending on the selected alkali metal type, the operating temperature, the pump and probe lasers' wavelengths, etc. are determined. Cs as an example of alkali metals, can be preferred in terms of low temperature and low power consumption, as it has a higher atomic density at lower temperatures in atomic spectroscopy and sensor applications [45–50]. However, a disadvantage of Cs alkali metal is that its alkali spin relaxation rate is much faster than the others [51]. Accordingly, Table 2 shows the operating temperatures in various experiments using Cs, Rb, and K alkali metals.

4.1. Alkali metal and noble gas

Alkali metal vapor is utilized in the SERF regime to polarize noble gas atoms and accurately measure their precession [27, 29]. Noble gases are also polarized using the spin exchange optical pumping (SEOP) method after the atoms of alkali metals have been polarized [62]. Applications for polarized noble gases include medical diagnostics, atomic gyroscopes, etc. [13, 63]. The alkali metal species K, Rb, and Cs are combined with the noble gases ^{3}He, ^{21}Ne, and ^{129}Xe in the CG's vapor cell. For instance, Table 2 lists the standard vapor cell content combinations for CG and shows alkali and noble gas types, the experimental setup's temperature, bias stability, angle random walk, and the publication year of the related paper. If there is no information about one of these parameters, "not available" (n.a.) is used. Early research especially preferred ^{3}He and ^{129}Xe. The lower gyromagnetic ratio of the noble gas ^{21}Ne enables higher sensitivity when used with alkali metals like K, Rb, or Cs [64, 65]. In contrast to other noble gases, the polarization of ^{21}Ne atoms is time-consuming and difficult [66]. In addition, when the noble gas ^{21}Ne was polarized with the alkali metals K and Rb, the measurement of spin-exchange and spin-relaxation parameters was examined. The results show that better sensitivity can be achieved using ^{21}Ne instead of ^{3}He [64]. Running CGs at low temperatures such as 110 °C

not only saves power but also makes it possible to manufacture paraffin-coated cells, which makes CGs more sensitive [67]. The circularly polarized pump laser polarizes optically thinner K alkali atoms along the pump axis. Through spin-exchange interactions with polarized K atoms, the relatively thicker Rb atoms get polarized. Spin-exchange collisions with the polarized K and Rb alkali metals cause ^{21}Ne atoms to become hyperpolarized as a result [68]. Hybrid optical pumping is being used to increase both the pumping efficiency of noble gases and the homogeneity of polarization of alkali metals [69, 70]. The CG steady-state output model has been developed analytically by taking into consideration two alkali metals and one noble gas species for optimization purposes [41], as the existing performances of CGs are far from theoretical limitations [13, 71]. Rb and K atoms act as if they were single alkali metal species because the rate of spin exchange between them is substantially higher than the relaxation rates of alkali metal atoms [41].

Table 2. SERF comagnetometer gyroscopes.

Alkali metal	Noble gas	Temp. (°C)	Bias St. ($^\circ/h$)	ARW ($^\circ/h^{1/2}$)	Year	Reference
K	^{3}He	170	n.a.	5x10^{-7}	2005	[13]
Cs	^{129}Xe	110	n.a.	1.2x10^{-6}	2013	[52]
Rb	^{129}Xe	110	n.a.	n.a.	2014	[53]
Cs	^{129}Xe	110	7x10^{-5}	4.2x10^{-3}	2013	[54]
K-Rb	^{21}Ne	180	0.1	n.a.	2016	[55]
K-Rb	^{21}Ne	185	n.a.	2.1x10^{-8}	2016	[56]
K-Rb	^{21}Ne	200	1x10^{-2}	n.a.	2017	[57]
Cs	^{129}Xe	190	3.25	n.a.	2013	[58]
K-Rb	^{21}Ne	200	0.05	n.a.	2018	[36]
K-Rb	^{21}Ne	215	n.a.	4.6x10^{-7}	2016	[59]
K-Rb	^{21}Ne	160-200	5x10^{-4}	1x10^{-7}	2019	[60]
Rb	^{3}He-^{129}Xe	110-200	9x10^{-3}	3x10^{-6}	2018	[16, 61]
K	^{3}He	n.a.	2.5x10^{-7}	n.a.	2010	[32]
K-Rb	^{21}Ne	n.a.	1.8x10^{-7}	n.a.	2011	[31]

4.2. Lasers in CG

4.2.1. Polarizations and power density

To determine the change in atomic spin precession, Dehmelt [72] and Kimball [73] suggested measuring the laser's intensity as it passed through an alkali metal cell in 1957. Following that, Woodman et al. [74] reported the Faraday rotation effect of the linear polarized laser used in NMR gyroscope studies. It was more sensitive than the circularly polarized laser-based approach in detecting atomic spin precession signals. Subsequently, other groups [23, 29, 75] performed high-precision magnetic field and inertial measurements using the linear polarized laser sensing method. Although the pump and probe lasers are typically arranged perpendicular to perform alkali metal and noble gas polarization in CG [13, 55], a theoretical analysis of the biaxial gyroscope was also given in one of the later studies [76], and a single laser beam and a biaxial atomic spin CG have been introduced in a recent study [77]. The effect of pump laser power density on sensitivity in single alkali metal CG was examined using the analytical solution of Bloch's equations for electron and nuclear spin ensembles [42, 68]. Experimental results using hybrid optical pumping with two different types of alkali metals are presented to

show the impact of the pump laser power density on the output signal [56]. Although the CG was first presented as a single-axis inertial sensor to detect rotation [13].

4.2.2. Miniaturization and stabilization

Regarding SWaP (size, weight, and power) criteria, the miniaturization of CG as an atomic sensor is a very important research area [78, 79]. For this reason, the CG that can detect angular rotation in two orthogonal directions simultaneously using a single probe beam has been presented [36, 80]. Probe laser stabilization is also specifically used to reduce system noise and increase the signal-to-noise ratio. Because of this, photoelastic modulation [81], Faraday modulation [68], and acoustic-optical modulation (AOM) [82] methods are used. The correlation between the signal-to-noise ratio (SNR) and probe laser intensity in CG has been presented in the report [83] to determine the optimum probe laser intensity.

5. Main challenges

The four most fundamental types of CG errors are magnetic field gradients, atomic collisions, pump lasers, and probe lasers (including light shift, cross talk, etc.) [13, 84].

5.1. Magnetic field and gradients

The gradient of the magnetic field is one of the main reasons for systematic errors in CGs. Different species inside the atomic vapor cell may be located at different locations in the magnetic field due to variations in thermal diffusion [85], gravity [86], or polarization [87]. Different sorts of atoms may therefore experience various magnetic fields if there are magnetic field gradients in the CG. Precautions can be taken to compensate for the magnetic field gradients [87]. All of these methods may also show calibration errors because they depend on the size of the atomic vapor cell and other things. Frequency shifts caused by magnetic field gradients [88] may reduce CG performance as these are thought to be related to the gyromagnetic ratio [89]. A single species type CG has been proven to be more effective in suppressing errors caused by magnetic field gradients than CGs made up of many atomic species [87, 90]. Additionally, atomic CG from a single species may have stronger spin polarization and a higher SNR compared to CG from other samples [50]. Numerous theoretical techniques for the analysis of frequency shifts and spin relaxation based on magnetic field gradients become even more important in terms of CG performances [91]. According to research on the effects of temperature and magnetic field gradients in Rb-^{3}He-^{129}Xe CGs [87], the frequency shift happens to depend on the third power of the high-order magnetic field gradient. Second, it is demonstrated that frequency shifts happen when there is a temperature gradient because of the thermal diffusion effect [87]. One significant noise source that has an impact on CG performance (rotational accuracy, long-term stability, etc.) is how the CG reacts to the magnetic field [87, 92]. When the response of the K-Rb-^{21}Ne CG was investigated, an electron spin resonance of around 188 Hz was discovered for this purpose [61, 85]. The magnetic field compensation point is controlled closed-loop by locking into this resonance to set the K-Rb-^{21}Ne CG magnetic field suppression factor [61, 85]. A gyroscope operating in the SERF regime has also been reported to have a significant bias deviation of 0.02 $^{\circ}/h$ due to magnetic field changes [93]. According to reports, magnetic noise has the biggest and most constraining impact on bias stability in CG [17, 50, 94]. A method for reducing the noble gas pressure and suppressing the transverse relaxation rate of nuclear spins was proposed [16]. Low bandwidth, which will limit applicability, has also been observed to result from low noble gas pressure. Due to this, when the cell temperature was examined, it was

found that increasing the temperature also increased CG bandwidth but decreased bias sensitivity [95]. The system's long-term stability will be impacted by deviation errors specifically caused by magnetic field changes in the direction of the magnetometer's probe laser. An in-situ measurement method has been proposed for this issue [96]. Magnetic noise generated by the shielding material because of Johnson current is another type of noise in CG [97]. Kornack et al. computed the magnetic shielding noise using equivalent power dissipation theory, and they discovered that conductivity, permeability, and size were the primary contributing factors [98].

5.2. Other effects

To improve CG sensitivity, the nuclear spin relaxation time and alkali metal atom density need to be measured which are the main limiting parameters [29]. The CG sensitivity and spin coherence time are controlled by the nuclear longitudinal spin relaxation rate (T1). The transverse relaxation ratio (T2) determines the dynamic response of nuclear spins. In summary, the time T1 is the upper limit of T2 [99]. The Polarization growth method [99], the single scan pulse sequence (ssps) [100], and free induction decay (FID) [101] are the current methods for calculating T1 time. One of the main sources of error in atomic vapor cells is light shifts [102]. As a result of light shifting, a virtual magnetic field forms, causing errors in light frequency and intensity [103]. In CG, these light shifts not only affect linewidth and sensitivity but also cause a crosstalk effect between two sensitive axes [55, 102]. It has been proposed that the light shift in the CG can be suppressed by selecting the ideal temperature of the vapor cell [104]. Walker's group used pulse modulation in NMR comagnetometers to improve long-term stability and minimize fluctuation caused by longitudinal polarization [105]. To improve CG performance, the pulse response model was presented [106]. When the effects of K-Rb hybrid cells on CG were examined, it was determined that by optimizing the vapor cell's density ratio and optical power density, the maximum output signal was attained [107]. A closed-loop laser power control system is often used in CGs to reduce errors caused by laser power. A method has been proposed for laser power stabilization by optimizing the ratio of the in-cycle laser power to the out-of-cycle laser power, thanks to the proposed split ratio optimization [108]. Errors caused by heating types in CGs were analyzed by comparing electric heating and laser heating methods [109]. Therefore, it has been reported that heating with a laser is more effective and stable at all temperatures that have been measured.

6. Conclusion

In this review, historical and technological developments, possible application areas, research topics, error types, and optimization options for CG are presented. The evolution of the technology, milestones, and application options are reported. The composition, technical background, and self-compensation mechanism of CG are introduced using the experimental setup scheme. The simulation of SERF CGs is carried out using a sample scenario with the necessary parameters. Related studies in the literature were compiled and basic compositions of CGs were presented. Important challenges to the performance of CGs are studied. Thus, it is aimed at contributing to the acceleration of studies to be carried out in this field by encouraging further research and providing a guide for researchers to develop high-precision gyroscope sensors.

References

[1] Tazartes D. An historical perspective on inertial navigation systems. In: 2014 international symposium on inertial sensors and systems (ISISS);Laguna Beach, CA, USA; 2014.1-5. doi: 10.1109/ISISS.2014.6782505

[2] Feng D. Review of quantum navigation. In: IOP Conference Series: Earth and Environmental Science 2019; 237(032027). doi: 10.1088/1755-1315/237/3/032027

[3] El-Sheimy N, Youssef A. Inertial sensors technologies for navigation applications: State of the art and future trends. Satellite Navigation 2020; 1 (1):1-21. doi: 10.1186/s43020-019-0001-5

[4] Bulatowicz M, Griffith R, Larsen M, Mirijanian J, Fu CB et al. Laboratory search for a long-range t-odd, p-odd interaction from axionlike particles using dual-species nuclear magnetic resonance with polarized xe 129 and xe 131 gas. Physical review letters 2013; 111 (10): 102001. doi: https://doi.org/10.48550/arXiv.1301.5224

[5] Wang Z, Zhao M, Yang J. A piezoelectric gyroscope with self-equilibrated coriolis force based on overtone thickness-shear modes of a lithium niobate plate with an inversion layer. IEEE Sensors Journal 2014; 15 (3): 1794-9. doi: 10.1109/JSEN.2014.2366235

[6] Everitt CF, DeBra DB, Parkinson BW, Turneaure JP, Conklin JW et al. Gravity probe B: final results of a space experiment to test general relativity. Physical Review Letters 2011; 106 (22): 221101. doi: https://doi.org/10.48550/arXiv.1105.3456

[7] Stedman GE. Ring-laser tests of fundamental physics and geophysics. Reports on progress in physics 1997; 60 (6): 615. doi: 10.1088/0034-4885/60/6/001

[8] Liu Y, Shi M, Wang X. Progress on atomic gyroscope. In: 2017 24th Saint Petersburg International Conference on Integrated Navigation Systems (ICINS);Saint Petersburg, Russia; 2017. pp. 1-7. doi: https://doi.org/10.23919/ICINS.2017.7995640

[9] Cronin AD, Schmiedmayer J, Pritchard DE. Optics and interferometry with atoms and molecules. Reviews of Modern Physics 2009; 81 (3): 1051. doi: https://doi.org/10.1103/RevModPhys.81.1051

[10] Liu WM, Wu B, Niu Q. Nonlinear effects in interference of Bose-Einstein condensates. Physical review letters 2000; 84 (11): 2294. doi: https://doi.org/10.1103/PhysRevLett.84.2294

[11] Degen CL, Reinhard F, Cappellaro P. Quantum sensing. Reviews of modern physics 2017; 89 (3): 035002. doi: https://doi.org/10.1103/RevModPhys.89.035002

[12] Meyer D, Larsen M. Nuclear magnetic resonance gyro for inertial navigation. Gyroscopy and Navigation 2014; 5 (2): 75-82. doi: https://doi.org/10.1134/S2075108714020060

[13] Kornack TW, Ghosh RK, Romalis MV. Nuclear spin gyroscope based on an atomic comagnetometer. Physical Review Letters 2005; 95 (23): 230801. doi: https://doi.org/10.1103/PhysRevLett.95.230801

[14] Donley EA. Nuclear magnetic resonance gyroscopes. IEEE SENSORS 2010; pp. 17-22. doi: https://doi.org/10.1109/ICSENS.2010.5690983

[15] Larsen M, Bulatowicz M. Nuclear Magnetic Resonance Gyroscope: For DARPA's micro-technology for positioning, navigation and timing program. In: 2012 IEEE International Frequency Control Symposium Proceedings; Baltimore, MD, USA; 2012. pp. 1-5. doi: https://doi.org/10.1109/ISISS.2014.6782506

[16] Fan W, Quan W, Liu F, Xing L, Liu G. Suppression of the bias error induced by magnetic noise in a spin-exchange relaxation-free gyroscope. IEEE Sensors Journal 2019; 19 (21): 9712-21. doi: https://doi.org/10.1109/JSEN.2019.2929505

[17] Liu Y, Gao H, Ma L, Quan J, Fan W et al. Study on the Magnetic Noise Characteristics of Amorphous and Nanocrystalline Inner Magnetic Shield Layers of SERF Co-Magnetometer. Materials 2022; 15 (22): 8267. doi: https://doi.org/10.3390/ma15228267

[18] Zhang K, Du P, Duan L, Cai Z, Yuan L et al. Closed-loop control of the longitudinal axis compensation point in the K-Rb-21Ne comagnetometer. Results in Physics 2023; 51: 106734. doi: https://doi.org/10.1016/j.rinp.2023.106734

[19] Wu J, Liu F, Fan W, Du P, Quan W. Temperature compensation methods of spin-exchange relaxation-free co-magnetometer. Measurement Science and Technology 2022; 34 (1): 015113. doi: https://doi.org/10.1088/1361-6501/ac97b0

[20] Knappe S, Schwindt PD, Shah V, Hollberg L, Kitching J et al. A chip-scale atomic clock based on 87 Rb with improved frequency stability. Optics express 2005; 13 (4): 1249-53. doi: https://doi.org/10.1364/OPEX.13.001249

[21] Mitchell M. Deliverable D6. 5 SERF-gyroscope feasibility report 2021

[22] Fertig C, Gibble K. Measurement and cancellation of the cold collision frequency shift in an 87 Rb fountain clock. Physical review letters 2000; 85 (8): 1622. doi: https://doi.org/10.1103/PhysRevLett.85.1622

[23] Kominis IK, Kornack TW, Allred JC, Romalis MV. A subfemtotesla multichannel atomic magnetometer. Nature 2003; 422 (6932): 596-9. doi: https://doi.org/10.1038/nature01484

[24] Dimopoulos S, Graham PW, Hogan JM, Kasevich MA. Testing general relativity with atom interferometry. Physical review letters 2007; 98 (11): 111102. doi: https://doi.org/10.48550/arXiv.gr-qc/0610047

[25] Neumann P, Jakobi I, Dolde F, Burk C, Reuter R et al. High-precision nanoscale temperature sensing using single defects in diamond. Nano letters 2013; 13 (6): 2738-42. doi: https://doi.org/10.1021/nl401216y

[26] Brinkmann D. Kernresonanz im gasförmigen Xenon. Kehrer, Freiburg i. Br.; 1962.

[27] Happer W, Tang H. Spin-exchange shift and narrowing of magnetic resonance lines in optically pumped alkali vapors. Physical Review Letters 1973; 31 (5): 273. doi: https://doi.org/10.1103/PhysRevLett.31.273

[28] Happer W, Tam AC. Effect of rapid spin exchange on the magnetic-resonance spectrum of alkali vapors. Physical Review A 1977; 16 (5): 1877. doi: https://doi.org/10.1103/PhysRevA.16.1877

[29] Allred J, Lyman RN, Kornack TW, Romalis MV. High-sensitivity atomic magnetometer unaffected by spin-exchange relaxation. Physical review letters 2002; 89 (13): 130801. doi: https://10.1103/PhysRevLett.89.130801

[30] Savukov IM, Romalis MV. Effects of spin-exchange collisions in a high-density alkali-metal vapor in low magnetic fields. Physical Review A 2005; 71 (2): 023405. doi: https://doi.org/10.1103/PhysRevA.71.023405

[31] Smiciklas M, Brown JM, Cheuk LW, Smullin SJ, Romalis MV. New Test of Local Lorentz Invariance Using a Ne 21− Rb− K Comagnetometer. Physical review letters 2011; 107 (17): 171604. doi: https://doi.org/10.1103/PhysRevLett.107.171604

[32] Brown JM, Smullin SJ, Kornack TW, Romalis MV. New limit on lorentz-and C P T-violating neutron spin interactions. Physical review letters 2010; 105 (15): 151604. doi: https://doi.org/10.48550/arXiv.1006.5425

[33] Härle P, Wäckerle G, Mehring M. A nuclear-spin based rotation sensor using optical polarization and detection methods. Applied Magnetic Resonance 1993; 5: 207-20. doi: https://doi.org/10.1007/BF03162522

[34] Braine T, Cervantes R, Crisosto N, Du N, Kimes S et al. Extended search for the invisible axion with the axion dark matter experiment. Physical review letters 2020; 124 (10): 101303. doi: https://doi.org/10.48550/arXiv.1910.08638

[35] Kitching J, Knappe S, Donley EA. Atomic sensors–a review. IEEE Sensors Journal 2011; 11 (9): 1749-58. doi: https://doi.org/10.1109/JSEN.2011.2157679

[36] Jiang L, Quan W, Li R, Fan W, Liu F et al. A parametrically modulated dual-axis atomic spin gyroscope. Applied Physics Letters 2018; 112 (5). doi: https://doi.org/10.1063/1.5018015

[37] Bloch F. Nuclear induction. Physical review 1946; 70 (7-8): 460. doi: https://doi.org/10.1103/PhysRev.70.460

[38] Liu J, Jiang L, Liang Y, Li G, Cai Z et al. Dynamics of a spin-exchange relaxation-free comagnetometer for rotation sensing. Physical Review Applied 2022; 17 (1): 014030. doi: https://doi.org/10.1103/PhysRevApplied.17.014030

[39] Jiang L, Quan W, Liu F, Fan W, Xing L et al. Closed-loop control of compensation point in the K− Rb− 21 Ne comagnetometer. Physical Review Applied 2019; 12 (2): 024017. doi: https://doi.org/10.48550/arXiv.1901.02683

[40] Karabinaoğlu MS, Koç E, Çakır B. Magnetic Shielding Simulation for a Low Noise Atomic Comagnetometer. In: 2023 10th International Conference on Electrical and Electronics Engineering (ICEEE) 2023; (pp. 327-332). doi: 10.1109/ICEEE59925.2023.00066

[41] Jiang L, Quan W, Liang Y, Liu J, Duan L et al. Effects of pump laser power density on the hybrid optically pumped comagnetometer for rotation sensing. Optics Express 2019; 27 (20): 27420-30. doi: https://doi.org/10.1364/OE.27.027420

[42] Brown JM. A new limit on lorentz-and cpt-violating neutron spin interactions using a potassium-helium comagnetometer. Princeton university 2011. doi: https://doi.org/10.48550/arXiv.1006.5425

[43] Schaefer SR, Cates GD, Chien TR, Gonatas D, Happer W et al. Frequency shifts of the magnetic-resonance spectrum of mixtures of nuclear spin-polarized noble gases and vapors of spin-polarized alkali-metal atoms. Physical Review A 1989; 39 (11): 5613. doi: https://doi.org/10.1103/PhysRevA.39.5613

[44] Tang C, Liu C, Prado CA, Zhao T, Han B et al. Design of real time magnetic field compensation system based on fuzzy PI control algorithm for comagnetometer. Journal of Physics D: Applied Physics 2022; 55(35): 355106. doi: https://doi.org/10.1088/1361-6463/ac6f99

[45] Babcock ED. Spin-exchange optical pumping with alkali-metal vapors. PhD, The University of Wisconsin-Madison, 2005.

[46] Fang J, Li R, Duan L, Chen Y, Quan W. Study of the operation temperature in the spin-exchange relaxation free magnetometer. Review of Scientific Instruments 2015; 86 (7). doi: https://doi.org/10.1063/1.4927460

[47] Chen Y, Zhao L, Zhang N, Yu M, Ma Y et al. Single beam Cs-Ne SERF atomic magnetometer with the laser power differential method. Optics Express 2022; 30 (10): 16541-52. doi: https://doi.org/10.1364/OE.450571

[48] Zhang DW, Xu ZY, Zhou M, Xu XY. Parameter analysis for a nuclear magnetic resonance gyroscope based on 133Cs–129Xe/131Xe. Chinese Physics B. 2017;26 (2):023201. doi: https://doi.org/10.1088/1674-1056/26/2/023201

[49] Ding Y, Xiao W, Zhao Y, Wu T, Peng X et al. Dual-Species All-Optical Magnetometer Based on a Cs-K Hybrid Vapor Cell. Physical Review Applied 2023; 21: 19 (3): 034066. https://doi.org/10.1103/PhysRevApplied.19.034066

[50] Yang Y, Wu T, Chen J, Peng X, Guo H. All-optical single-species cesium atomic comagnetometer with optical free induction decay detection. Applied Physics B 2021; 127: 1-1. doi: https://doi.org/10.1007/s00340-021-07594-w

[51] Zeng X, Wu Z, Call T, Miron E, Schreiber D et al. Experimental determination of the rate constants for spin exchange between optically pumped K, Rb, and Cs atoms and Xe 129 nuclei in alkali-metal–noble-gas van der Waals molecules. Physical Review A 1985; 31(1): 260. doi: https://doi.org/10.1103/PhysRevA.31.260

[52] Fang J, Wan S, Yuan H. Dynamics of an all-optical atomic spin gyroscope. Applied optics 2013; 52(30): 7220-7. doi: https://doi.org/10.1364/AO.52.007220

[53] Renon G, Zahzam N, Bidel Y, Bresson A, Nacher PJ. A nuclear-electronic spin gyro-comagnetometer. In: APS division of atomic, molecular and optical physics meeting abstracts 2014; pp. M6-002.

[54] Fang J, Qin J, Wan S, Chen Y, Li R. Atomic spin gyroscope based on 129 Xe-Cs comagnetometer. Chinese Science Bulletin 2013; 58: 1512-5. doi: https://doi.org/10.1007/s11434-013-5759-5

[55] Li R, Fan W, Jiang L, Duan L, Quan W et al. Rotation sensing using a K-Rb-Ne 21 comagnetometer. Physical Review A 2016; 94 (3): 032109. doi: https://doi.org/10.1103/PhysRevA.94.032109

[56] Chen Y, Quan W, Zou S, Lu Y, Duan L et al. Spin exchange broadening of magnetic resonance lines in a high-sensitivity rotating K-Rb-21Ne co-magnetometer. Scientific reports 2016; 6 (1): 36547. doi: https://doi.org/10.1038/srep36547

[57] Jiang L, Quan W, Li R, Duan L, Fan W et al. Suppression of the cross-talk effect in a dual-axis K− Rb− Ne 21 comagnetometer. Physical Review A 2017; 95 (6): 062103. doi: https://doi.org/10.1103/PhysRevA.95.062103

[58] Fang J, Wan S, Qin J, Zhang C, Quan W et al. A novel Cs-129Xe atomic spin gyroscope with closed-loop Faraday modulation. Review of Scientific Instruments 2013; 84(8). doi: https://doi.org/10.1063/1.4819306

[59] Fang J, Chen Y, Zou S, Liu X, Hu Z et al. Low frequency magnetic field suppression in an atomic spin comagnetometer with a large electron magnetic field. Journal of Physics B: Atomic, Molecular and Optical Physics 2016; 49 (6): 065006. doi: https://doi.org/10.1088/0953-4075/49/6/065006

[60] Fan W, Quan W, Zhang W, Xing L, Liu G. Analysis on the magnetic field response for nuclear spin co-magnetometer operated in spin-exchange relaxation-free regime. IEEE Access 2019; 7: 28574-80. doi: https://doi.org/10.1109/ACCESS.2019.2902181

[61] Limes ME, Sheng D, Romalis MV. He 3− Xe 129 comagnetometery using Rb 87 detection and decoupling. Physical review letters 2018; 120 (3): 033401. doi: https://doi.org/10.1103/PhysRevLett.120.033401

[62] Walker TG, Happer W. Spin-exchange optical pumping of noble-gas nuclei. Reviews of modern physics 1997; 69 (2): 629. doi: https://doi.org/10.1103/RevModPhys.69.629

[63] Oros AM, Shah NJ. Hyperpolarized xenon in NMR and MRI. Physics in Medicine Biology 2004; 49 (20): R105. doi: https://doi.org/10.1088/0031-9155/49/20/r01

[64] Ghosh RK, Romalis MV. Measurement of spin-exchange and relaxation parameters for polarizing Ne 21 with K and Rb. Physical Review A 2010; 81 (4): 043415. doi: https://doi.org/10.1103/PhysRevA.81.043415

[65] Quan W, Wei K, Li H. Precision measurement of magnetic field based on the transient process in a K-Rb-21 Ne co-magnetometer. Optics Express 2017; 25 (8): 8470-83. doi: https://doi.org/10.1364/OE.25.008470

[66] Shi M. Investigation on magnetic field response of a 87Rb-129Xe atomic spin comagnetometer. Opt. Express 2020; 32033-32041. doi: https://doi.org/10.1364/OE.404809

[67] Ledbetter MP, Savukov IM, Acosta VM, Budker D, Romalis MV. Spin-exchange-relaxation-free magnetometry with Cs vapor. Physical Review A 2008; 77 (3): 033408. doi: https://doi.org/10.1103/PhysRevA.77.033408

[68] Kornack TW. A test of CPT and Lorentz symmetry using a potassium-helium-3 co-magnetometer. Princeton University; 2005.

[69] Chen WC, Gentile TR, Walker TG, Babcock E. Spin-exchange optical pumping of He 3 with Rb-K mixtures and pure K. Physical Review A 2007; 75 (1): 013416. doi: https://doi.org/10.1103/PhysRevA.75.013416

[70] Romalis MV. Hybrid optical pumping of optically dense alkali-metal vapor without quenching gas. Physical review letters 2010; 105 (24): 243001. doi: https://doi.org/10.1103/PhysRevLett.105.243001

[71] Zhang C, Yuan H, Tang Z, Quan W, Fang JC. Inertial rotation measurement with atomic spins: From angular momentum conservation to quantum phase theory. Applied Physics Reviews 2016; 3 (4). doi: https://doi.org/10.1063/1.4972187

[72] Dehmelt HG. Modulation of a light beam by precessing absorbing atoms. Physical Review 1957; 105 (6): 1924. doi: https://doi.org/10.1103/PhysRev.105.1924

[73] Kimball DF, Jacome LR, Guttikonda S, Bahr EJ, Chan LF. Magnetometric sensitivity optimization for nonlinear optical rotation with frequency-modulated light: Rubidium D2 line. Journal of Applied Physics 2009; 106 (6). doi: https://doi.org/10.48550/arXiv.0906.3586

[74] Woodman KF, Franks PW, Richards MD. The nuclear magnetic resonance gyroscope: a review. The Journal of Navigation 1987; 40 (3): 366-84. doi: https://doi.org/10.1017/S037346330000062X

[75] Kornack TW, Romalis MV. Dynamics of two overlapping spin ensembles interacting by spin exchange. Physical review letters 2002; 89 (25): 253002. doi: https://doi.org/10.1103/PhysRevLett.89.253002

[76] Cai Q, Yang G, Quan W, Song N, Tu Y et al. Error analysis of the K-Rb-21Ne comagnetometer space-stable inertial navigation system. Sensors 2018; 18 (2): 670. doi: https://doi.org/10.3390/s18020670

[77] Jiang L, Liu J, Liang Y, Tian M, Quan W. A single-beam dual-axis atomic spin comagnetometer for rotation sensing. Applied Physics Letters 2022; 120 (7). doi: https://doi.org/10.1063/5.0079429

[78] Liew LA, Knappe S, Moreland J, Robinson H, Hollberg L, Kitching J. Microfabricated alkali atom vapor cells. Applied Physics Letters 2004; 84 (14): 2694-6. doi: https://doi.org/10.1063/1.1691490

[79] Mhaskar R, Knappe S, Kitching J. A low-power, high-sensitivity micromachined optical magnetometer. Applied Physics Letters 2012; 101 (24). doi: https://doi.org/10.1063/1.4770361

[80] Li Z, Wakai RT, Walker TG. Parametric modulation of an atomic magnetometer. Applied physics letters 2006; 89 (13). doi: https://doi.org/10.1063/1.2357553

[81] Duan L, Fang J, Li R, Jiang L, Ding M et al. Light intensity stabilization based on the second harmonic of the photoelastic modulator detection in the atomic magnetometer. Optics Express 2015; 23 (25): 32481-9. doi: https://doi.org/10.1364/OE.23.032481

[82] Xing L, Zhai Y, Fu Y, Song T, Liu F et al. Optical rotation detection method based on acousto-optic modulation in an atomic spin co-magnetometer. Measurement Science and Technology 2020; 32 (2): 025112. doi: https://doi.org/10.1088/1361-6501/abbc8a

[83] Fu Y, Fan W, Ruan J, Liu Y, Lu Z et al. Effects of probe laser intensity on co-magnetometer operated in spin-exchange relaxation-free regime. IEEE Transactions on Instrumentation and Measurement 2022; 71: 1-7. doi: https://doi.org/10.1109/TIM.2022.3144738

[84] Pang H, Liu F, Fan W, Wu Z, Yuan Q et al. Comprehensive analysis of the effects of magnetic field gradient on the performance of the SERF co-magnetometer. Optics Express 2023;31 (4): 5215-28. doi: https://doi.org/10.1364/OE.478875

[85] Ledbetter MP, Pustelny S, Budker D, Romalis MV, Blanchard JW et al. Liquid-state nuclear spin comagnetometers. Physical review letters 2012; 108 (24): 243001. doi: https://doi.org/10.1103/PhysRevLett.108.243001

[86] Baker CA, Doyle DD, Geltenbort P, Green K, Van der Grinten MG et al. Improved experimental limit on the electric dipole moment of the neutron. Physical review letters 2006; 97 (13): 131801. doi: https://doi.org/10.1103/PhysRevLett.97.131801

[87] Sheng D, Kabcenell A, Romalis MV. New classes of systematic effects in gas spin comagnetometers. Physical review letters 2014; 113 (16): 163002. doi: https://doi.org/10.1103/PhysRevLett.113.163002

[88] Cates GD, Schaefer SR, Happer W. Relaxation of spins due to field inhomogeneities in gaseous samples at low magnetic fields and low pressures. Physical review A 1988; 37 (8): 2877. doi: https://doi.org/10.1103/PhysRevA.37.2877

[89] Pendlebury JM, Heil W, Sobolev Y, Harris PG, Richardson JD et al. Geometric-phase-induced false electric dipole moment signals for particles in traps. Physical Review A 2004; 70 (3): 032102. doi: https://doi.org/10.1103/PhysRevA.70.032102

[90] Kimball DF, Lacey I, Valdez J, Swiatlowski J, Rios C et al. A dual-isotope rubidium comagnetometer to search for anomalous long-range spin-mass (spin-gravity) couplings of the proton. Annalen der Physik 2013; 525 (7): 514-28. doi: https://doi.org/10.48550/arXiv.1304.4660

[91] Zheng W, Gao H, Liu JG, Zhang Y, Ye Q et al. General solution to gradient-induced transverse and longitudinal relaxation of spins undergoing restricted diffusion. Physical Review A 2011; 84 (5): 053411. doi: https://doi.org/10.1103/PhysRevA.84.053411

[92] Tullney K, Allmendinger F, Burghoff M, Heil W, Karpuk S et al. Constraints on spin-dependent short-range interaction between nucleons. Physical review letters 2013; 111 (10): 100801. doi: https://doi.org/10.48550/arXiv.1303.6612

[93] Li R, Quan W, Fan W, Xing L, Fang J. Influence of magnetic fields on the bias stability of atomic gyroscope operated in spin-exchange relaxation-free regime. Sensors and Actuators A: Physical 2017; 266: 130-4. doi: https://doi.org/10.1016/j.sna.2017.09.023

[94] Fan W, Quan W, Liu F, Pang H, Xing L et al. Performance of low-noise ferrite shield in a k-rb-21 ne comagnetometer. IEEE Sensors Journal 2019; 20 (5): 2543-9. doi: https://doi.org/10.1109/JSEN.2019.2952121

[95] Fan W, Duan L, Huang J, Zhang W, Quan W. Effect of cell temperature on the bias magnetic sensitivity of an atomic spin co-magnetometer. In AOPC 2020: Optoelectronics and Nanophotonics; and Quantum Information Technology 2020; Vol. 11564, pp. 123-127. doi: https://doi.org/10.1117/12.2575681

[96] Huang J, Wang Z, Fan W, Pang H, Zhang K et al. In-situ evaluation of low-frequency magnetic field fluctuation in an atomic comagnetometer. IEEE Sensors Journal 2021; 21 (20): 22846-52. doi: https://doi.org/10.1109/JSEN.2021.3106899

[97] Lu J, Ma D, Yang K, Quan W, Zhao J et al. Study of magnetic noise of a multi-annular ferrite shield. IEEE Access 2020; 8: 40918-24. doi: https://doi.org/10.1109/ACCESS.2020.2976785

[98] Kornack TW, Smullin SJ, Lee SK, Romalis MV. A low-noise ferrite magnetic shield. Applied physics letters 2007; 90 (22). doi: https://doi.org/10.1063/1.2737357

[99] Mirijanian JJ. Techniques to characterize vapor cell performance for a nuclear-magnetic-resonance gyroscope. California Polytechnic State University; 2012. doi: https://doi.org/10.15368/theses.2012.39

[100] Loening NM, Thrippleton MJ, Keeler J, Griffin RG. Single-scan longitudinal relaxation measurements in high-resolution NMR spectroscopy. Journal of Magnetic Resonance 2003; 164 (2): 321-8. doi: https://doi.org/10.1016/s1090-7807(03)00186-1

[101] Savukov IM, Romalis MV. NMR detection with an atomic magnetometer. Physical review letters 2005; 94 (12): 123001. doi: https://doi.org/10.1103/PhysRevLett.94.123001

[102] Li Y, Ding M, Liu X, Cai H, Zhao J et al. Suppression method of AC-stark shift in SERF atomic magnetometer. IEEE Photonics Journal 2018; 10 (5): 1-7. doi: https://doi.org/10.1109/JPHOT.2018.2872026

[103] Fang J, Wan S, Chen Y, Li R. Light-shift measurement and suppression in atomic spin gyroscope. Applied Optics 2012; 51 (31): 7714-7. doi: https://doi.org/10.1364/AO.51.007714

[104] Liu F, Duan L, Fan W, Pang H, Liu S et al. Suppression method of light shift in K-Rb hybrid optical pumping SERF atomic comagnetometer. IEEE Sensors Journal 2021; 21 (23): 26665-72. doi: https://doi.org/10.1109/JSEN.2021.3122990

[105] Thrasher DA, Sorensen SS, Weber J, Bulatowicz M, Korver A et al. Continuous comagnetometry using transversely polarized Xe isotopes. Physical Review A 2019; 100 (6): 061403. doi: https://doi.org/10.48550/arXiv.1910.02156

[106] Liu J, Jiang L, Liang Y, Tian M, Quan W. Investigation on the pulse response of a spin-exchange relaxation-free comagnetometer. Optics Express 2022; 30 (14): 25509-21. doi: https://doi.org/10.1364/OE.462795

[107] Zhao T, Zhai Y, Liu C, Xie H, Cao Q et al. Spin polarization characteristics of hybrid optically pumped comagnetometers with different density ratios. Optics Express 2022; 30 (15): 28067-78. doi: https://doi.org/10.1364/OE.463651

[108] Zhang WJ, Fan WF, Fan SM, Quan W. Suppression of laser power error in a miniaturized atomic co-magnetometer based on split ratio optimization. Chinese Physics B 2023; 32 (3): 030701. doi: https://doi.org/10.1088/1674-1056/ac81b1

[109] Zhao T, Liu Y, Wei K, Xie H, Mu T et al. Ultra-sensitive all-optical comagnetometer with laser heating. Journal of Physics D: Applied Physics 2022; 55 (16): 165103. doi: https://doi.org/10.1088/1361-6463/ac49b5